

Numerical simulation study of ionization characteristics of argon dielectric barrier discharge

Guiming Liu(刘桂铭), Lei Chen(陈雷), Zhibo Zhao(赵智博), and Peng Song(宋鹏)
Citation: Chin. Phys. B, 2023, 32 (**12**): 125205. DOI: 10.1088/1674-1056/acc0f8
Journal homepage: http://cpb.iphy.ac.cn; http://iopscience.iop.org/cpb

What follows is a list of articles you may be interested in

Flow control performance evaluation of a tri-electrode sliding discharge plasma actuator

Borui Zheng(郑博睿), Yuanpeng Liu(刘园鹏), Minghao Yu(喻明浩), Yuanzhong Jin(金元中),Qian Zhang(张倩), and Quanlong Chen(陈全龙)
Chin. Phys. B, 2023, 32 (**9**): 095203. DOI: 10.1088/1674-1056/acae76

Dynamic stall control over an airfoil by NS-DBD actuation

He-Sen Yang(杨鹤森), Guang-Yin Zhao(赵光银)†, Hua Liang(梁华)‡, and Biao Wei(魏彪)
Chin. Phys. B, 2020, 29 (**10**): 105203. DOI: 10.1088/1674-1056/abb227

Electrical modeling of dielectric barrier discharge considering surface charge on the plasma modified material

Hong-Lu Guan(关弘路), Xiang-Rong Chen(陈向荣), Tie Jiang(江铁), Hao Du(杜浩), Ashish Paramane, Hao Zhou(周浩)
Chin. Phys. B, 2020, 29 (**7**): 075204. DOI: 10.1088/1674-1056/ab8a3f

Influence of vibration on spatiotemporal structure of the pattern in dielectric barrier discharge

Rong Han(韩蓉), Li-Fang Dong(董丽芳), Jia-Yu Huang(黄加玉), Hao-Yang Sun(孙浩洋), Bin-Bin Liu(刘彬彬), Yan-Lin Mi(米彦霖)
Chin. Phys. B, 2019, 28 (**7**): 075204. DOI: 10.1088/1674-1056/28/7/075204

Effect of actuating frequency on plasma assisted detonation initiation

Si-Yin Zhou(周思引), Xue-Ke Che(车学科), Di Wang(王迪), Wan-Sheng Nie(聂万胜)
Chin. Phys. B, 2018, 27 (**2**): 025208. DOI: 10.1088/1674-1056/27/2/025208

Numerical simulation study of ionization characteristics of argon dielectric barrier discharge

Guiming Liu(刘桂铭)[1], Lei Chen(陈雷)[1,†], Zhibo Zhao(赵智博)[2], and Peng Song(宋鹏)[2]

[1] *Liaoning Key Laboratory of Advanced Measurement and Test Technology for Aviation Propulsion System, Shenyang Aerospace University, Shenyang* 110136, *China*

[2] *College of Mechanical and Electrical Engineering, Dalian Minzu University, Dalian* 116600, *China*

(Received 17 January 2023; revised manuscript received 28 February 2023; accepted manuscript online 3 March 2023)

In order to better analyze the characteristics of particle distribution and its influencing factors in the ionized space during the process of coaxial dielectric barrier discharge, a self-designed two-dimensional axisymmetric structure exciter was used to carry out optical diagnosis, with the electron temperature calculated through Gaussian fitting. A plasma model was applied to conduct research on the discharge process through numerical simulation, with the changes in electron density and electron temperature were analyzed by using different discharge parameters. The research results show that with an increase in discharge voltage, pressure inside the reactor and relative permittivity, the discharge process is promoted. In addition, a rise in current density leads to an increase in the number of charged particles on the surface of the medium during the discharge process, while a rise in discharge intensity causes an increase in the electron density. Electron temperature decreases due to the increased loss of collision energy between particles. These results were confirmed by comparing experimental data with simulation results.

Keywords: dielectric barrier discharge, particle distribution properties, electron density, electron temperature

PACS: 52.80.Tn, 52.65.–y **DOI:** 10.1088/1674-1056/acc0f8

1. Introduction

According to some research, non-equilibrium plasmas are applicable in a wide range of fields such as medical services, aerospace, environmental protection and agricultural production.[1,2] They can be generated by glow discharge, corona discharge, dielectric barrier discharge (DBD) and so on.[3–5] Among various discharge technologies, DBD provides one of the most effective solutions to the generation of low-temperature non-equilibrium plasma under atmospheric pressure. Capable of working under high pressure and at a wide frequency range, it meets the requirement for use of plasma discharge technology under high pressures, playing an important role in the industrial application of low-temperature plasma.[6–8] Therefore, many scholars have already carried out research on how the characteristics of a DBD would be affected by the parameters of the DBD actuator structure, discharge parameters, working conditions and other factors.[9–11]

In the process of DBD, it is worth paying attention to the selection of dielectric materials, the structure of the discharge space and the size of the input voltage as these factors can affect the ionization characteristics of particles.[12] Judée *et al.*[13] compared the plasma parameters of the jet part of the exciter of a single dielectric layer DBD and a double dielectric layer DBD so as to analyze their ionization characteristics and the factors influencing plasma jet length and ionization velocity. However, no consideration was given to the law governing the influence of different parameters on the characteristics of ionization inside the exciter.[13] Barkaoui *et al.*[14] studied the effects of aerodynamic parameters and input voltage of gas on a plasma jet to analyze the effect of gas velocity on the electric field and electron density in the course of propagation. Despite this, no analysis was conducted on the characteristics of particle ionization in the exciter.[14] Bai *et al.*[15] investigated the thermodynamic reaction process of a nanosecond pulsed DBD to analyze how to produce important substances when methane and carbon dioxide are introduced, with the generation of these substances described in detail. However, little attention was paid to analyzing the final result of ionization.[15] Wang *et al.*[16] conducted a study on the characteristics of multi-current pulse dielectric layer discharge with a ring electrode under atmospheric pressure. In this study, the effects of different current pulses on ionization characteristics in the same cycle were described. They analyzed the patterns of variation in discharge mode, current density, electron density and electric field when the number of current pulses was changed. However, they did not take into account how the structural parameters of the physical model would affect the characteristics of ionization.[16] Wang *et al.*[17] used a one-dimensional fluid simulation model of a He/N_2 dielectric blocking discharge with parallel plate electrodes to investigate the law of the effect of different gap widths, secondary electron emission coefficients and driving frequencies on the characteristics of the multi-current pulse discharge and transition of the discharge mode. The process of discharge mode transition

†Corresponding author. E-mail: chenlei@sau.edu.cn

© 2023 Chinese Physical Society and IOP Publishing Ltd

was further explored when the parameters changed, but the effect on the particle discharge characteristics was ignored.[17] Apart from assisting the effort to establish the correlation between the structural parameters, working parameters and performance indices of the discharge exciter, the results of qualitative and quantitative analyses of the internal working process and its influencing factors also provide a crucial reference for the design and development of the discharge exciter and accelerate the development cycle. It is thus necessary to reveal the rationale of the DBD exciter and identify its influencing factors. In addition, simulation of the plasma must be performed progressively because setting the actual working conditions directly often leads to error and hampers troubleshooting. Given the relative simplicity of the reaction kinetics of Ar, we first study Ar in this paper to summarize the law applied to setting the practical conditions of simulation and application for reference.[18] However, most of the current plasma simulations are one-dimensional. Unlike two-dimensional simulations, they ignore the distribution of particles in the axial direction, which results in inaccurate simulation results.[19–21]

To solve this problem, the internal discharge process and operating characteristics of a DBD exciter are taken as the research object of this paper, with Ar as the carrier gas. The purpose is to explore the effect of different voltages, pressures inside the reactor and relative permittivities on the characteristics of ionization under atmospheric pressure. The distribution laws of electron density, potential and electron temperature are also analyzed. This helps address the shortcoming of one-dimensional simulations.

2. Experimental details

2.1. Experimental setup

The experimental setup is illustrated in Fig. 1. The plasma generator shown in the figure is a coaxial DBD device independently developed by our group. As its components, the central electrode is made of purple copper with a diameter of 7 mm and a length of 65 mm, the insulation layer is made of polytetrafluoroethylene (PTFE) with a relative dielectric constant of 2.55, the shell is made of 304 stainless steel with a discharge gap of 2 mm and the CPT-2000K low-temperature plasma power supply produced by Nanjing Suman is purposed to power the DBD device. The voltage and current waveforms generated during the experiment were recorded using a Tektronix-TDS1002 digital oscilloscope. A MX2500+ multichannel spectrometer was employed to record the spectral information and transmit the spectral data to the computer in real time, facilitating both observation and recording.

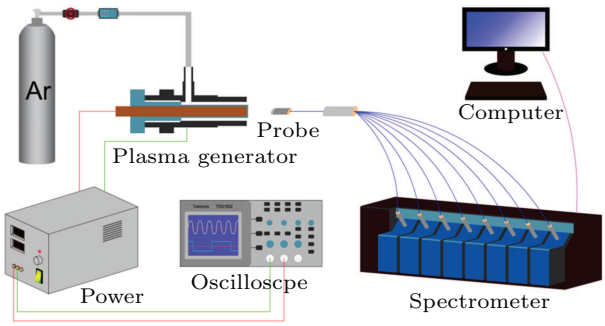


Fig. 1. Schematic diagram of the experimental setup.

2.2. Spectral diagnostic method and calculation of electron density

Figure 2 illustrates how spectral acquisition was performed. With the fiber optic probe fixed at a distance of 30 mm from the DBD device, the axis of the fiber optic probe and the DBD device were kept aligned during the experiment. Also, the spectral information on the plasma generated by the DBD was collected by the spectrometer.

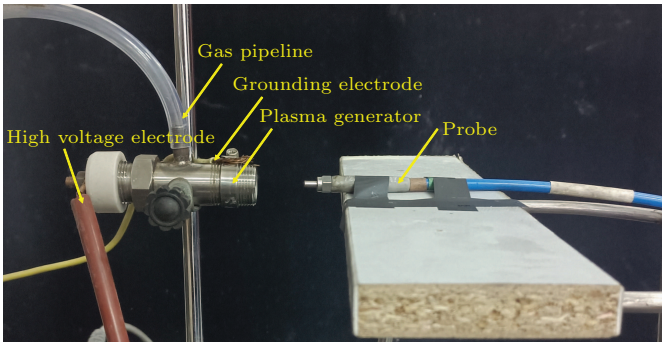


Fig. 2. Physical diagram of spectral acquisition.

For the spectral lines of non-hydrogen-like atoms, the Boltzmann slope method was used. For the two emission spectral lines at wavelengths λ_1 and λ_2, the ratio of their intensities is expressed as

$$\frac{I_1}{I_2} = \frac{\lambda_2}{\lambda_1}\frac{g_1 A_1}{g_2 A_2} \cdot \exp^{\frac{E_2 - E_1}{kT_e}}, \tag{1}$$

where I is the intensity of the emitted light, k is the Boltzmann constant, g is the statistical weight, A is the Einstein coefficient of the spontaneous radiation, E is the excitation energy of the spectral line and T_e is the electron excitation temperature. By taking logarithms for both sides of the above equation, the collation yield is obtained as

$$T_e = \frac{5040(E_1 - E_2)}{\ln\frac{A_1 g_1}{A_2 g_2} - \ln\frac{I_1}{I_2} - \ln\frac{\lambda_1}{\lambda_2}}, \tag{2}$$

where the values of excitation energy E are obtained from the atomic spectra database, g and A are obtained from the National Institute of Standards and Technology table of leap odds and the spectral intensity I is measured using a spectrometer. Thus, the electron excitation temperature can be calculated by measuring only the spectral intensities of the two emitted lights with wavelengths λ_1 and λ_2. To calculate the electron excitation temperature using Eq. (2), the following requirements need to be met. Firstly, the light emission of both

spectral lines must be proportional to the ground state Bourget number. Secondly, the two excited states undergo a known electron collisional excitation process. Thirdly, the leap is subjected to no radiative capture. Fourthly, the two excitation energies are basically identical. Fifthly, there is no variation in the leap probabilities and other de-activation steps of the two spectral lines with the change of the plasma. Lastly, the excitation processes of the two spectral lines are related to the electron energy at the same level. By introducing the natural logarithm of the intensity relationship of the emitted light and inputting the values of k, the following formula is obtained:

$$\ln\left(\frac{I\lambda}{gA}\right) = -\frac{5040}{T_{\mathrm{e}}}E + C. \tag{3}$$

According to Eq. (3), if a series of $\ln(I\lambda/(gA))$ values corresponding to the excitation energy E of each spectral line are plotted as coordinates, it is theoretically possible to obtain a straight line with a slope of $-5040/T_{\mathrm{e}}$. Thus, the electron excitation temperature T_{e} can be calculated.

3. Simulation model

3.1. Physical model

Figure 3 shows a three-dimensional model of the coaxial dielectric blocking discharge. As can be seen from the figure, the AC is connected to the central electrode, the dielectric layer covers the surface of the central electrode and the ground electrode is connected to the metal shell. The diameter of the central electrode is 2 mm, the thickness of the dielectric layer is 1 mm, the thickness of the metal shell is 1 mm and the discharge gap between the dielectric layer and the metal shell is 2 mm. PTFE is taken as the dielectric material, and has a relative dielectric constant of 2.55. A sinusoidal AC voltage is applied between the central electrode and the metal housing

$$U = 10000\,[\mathrm{V}] \times \sin(2\pi f_0 t). \tag{4}$$

The discharge frequency $f_0 = 10^4$ Hz. The discharge gap is filled with pure Ar gas, the temperature of which is set to 300 K, and the pressure inside the reactor is set to 1 atm. The initial electron density is set to 10^{10} m^{-3} and the initial average electron energy is set to 4 V. Due to the large computational volume of the actual three-dimensional model, the model is simplified into a two-dimensional axisymmetric model in this paper for improved efficiency of computation. Figure 4 shows the simulation model used in this study. According to the figure, the dielectric layer width $x = 1$ mm, the discharge gap $d = 2$ mm and the length $L = 8$ mm.

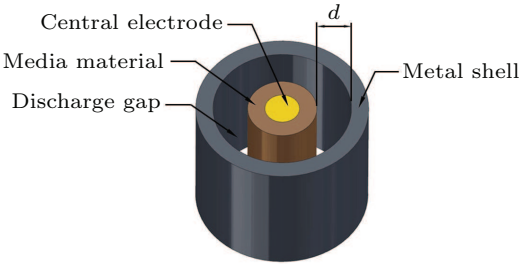


Fig. 3. Three-dimensional model of the coaxial medium blocking discharge.

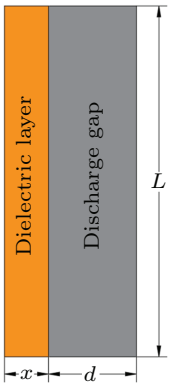


Fig. 4. Simulation model.

3.2. Chemical model

The kinetic reactions that occur when the dielectric barrier is infused with gas discharges are highly complex. At present, there remains a lack of clarity on the influence of the interactions between different particles on the results. The reaction kinetics of Ar plasma is far less complex than the reactions of gas in the ionization process. The mechanism of Ar plasma reaction is shown in Table 1, with four types of particles, namely, e, Ar, Ars and Ar^+, involved in a total of seven different reactions.

Table 1. Argon plasma reaction mechanism.

Reaction no.	Reaction	Collision type	Rate constant[a,b]	Energy loss $\Delta\varepsilon$ (eV)
1	$e + Ar \Rightarrow e + Ar$	elastic	k_{e1}	
2	$e + Ar \Rightarrow e + Ars$	excitation	k_{e2}	11.50
3	$e + Ars \Rightarrow e + Ar$	excitation	k_{e3}	–11.50
4	$e + Ar \Rightarrow 2e + Ar^+$	ionization	k_{e4}	15.80
5	$e + Ars \Rightarrow 2e + Ar^+$	ionization	k_{e5}	4.427
6	$Ars + Ars \Rightarrow e + Ar + Ar^+$	penning ionization	3.3734×10^8	
7	$Ars + Ar \Rightarrow Ar + Ar$	metastable quenching	1807	

[a]Rate coefficients k_{e1-5} are computed from the cross section σ and electron energy distribution function[22] and the unit is $m^3 \cdot s^{-1}$.
[b]Rate coefficients of reactions 6 and 7 are in units of $m^3 \cdot s^{-1} \cdot mol^{-1}$.

3.3. Mathematical models

The transport equations for electrons during the model calculation are formulated as follows:

$$\frac{\partial n_{\mathrm{e}}}{\partial t}+\nabla\cdot\Gamma_{\mathrm{e}}=R_{\mathrm{e}}-(u\cdot\nabla)n_{\mathrm{e}}, \tag{5}$$

$$\frac{\partial n_{\mathrm{e}}}{\partial t}+\nabla\cdot\Gamma_{\mathrm{e}}+E\cdot\Gamma_{\varepsilon}=R_{\varepsilon}-(u\cdot\nabla)n_{\varepsilon}, \tag{6}$$

where n_{e} and n_{ε} are the electron number density and electron energy density, E is the electric field strength in the discharge space, R_{e} is the electron rate expression, R_{ε} is the energy loss due to inelastic collisions, u is to the mass-averaged flow rate, Γ_{e} is the electron flux and Γ_{ε} is the electron energy. The R_{e} and R_{ε} are calculated as

$$R_{\mathrm{e}}=\sum_{j=1}^{M}c_j k_{\mathrm{e}j}N_{\mathrm{n}}n_{\mathrm{e}}, \tag{7}$$

$$R_{\varepsilon}=\sum_{j=1}^{M}c_j k_{\mathrm{e}j}N_{\mathrm{n}}n_{\mathrm{e}}\Delta\varepsilon_j, \tag{8}$$

where $k_{\mathrm{e}j}$ is the reaction rate coefficient, c_j is the molar concentration of reactants in the jth reaction, N_{n} is the number density of neutral particles and $\Delta\varepsilon_j$ is the energy loss during the reaction.

Based on the drift-diffusion approximation, the electron flux and energy flux are calculated as

$$\Gamma_{\mathrm{e}}=-(\mu_{\mathrm{e}}\cdot E)n_{\mathrm{e}}-D_{\mathrm{e}}\cdot\nabla n_{\mathrm{e}}, \tag{9}$$

$$\Gamma_{\varepsilon}=-(\mu_{\varepsilon}\cdot E)n_{\varepsilon}-D_{\varepsilon}\cdot\nabla n_{\varepsilon}, \tag{10}$$

where μ_{e} is the electron mobility, μ_{ε} is the electron energy mobility, D_{e} is the diffusion coefficient of electrons and D_{ε} is the energy diffusivity of electrons.

The electron temperature is calculated with the equation of conservation of electron energy

$$\frac{\partial n_{\varepsilon}}{\partial t}+\nabla\cdot\Gamma_{\varepsilon}=S_{\varepsilon}. \tag{11}$$

The electric field E is governed by Poisson's equation, which is related to the potential V

$$E=-\nabla V. \tag{12}$$

The boundary conditions for the electrons on the solid wall are

$$n_{\mathrm{e}}\cdot\Gamma_{\mathrm{e}}=\frac{1}{2}n_{\mathrm{e}}\sqrt{\frac{8kT_{\mathrm{e}}}{\pi n_{\mathrm{e}}}}-\alpha_{\mathrm{s}}\sum_{i}\gamma_i(\Gamma_i\cdot n)+\alpha'_{\mathrm{s}}\mu_i n_i E, \tag{13}$$

where n is the unit normal vector on the surface of the medium, γ_i is the secondary electron emission coefficient, α_{s} is the switching function associated with E and α'_{s} being the switching function associated with n.

4. Results and analysis

In this paper, finite element analysis is conducted to explore the discharge characteristics of a coaxial DBD. To begin with, the particle discharge process is studied under a specific working condition. Then, the effect on the particle distribution in the DBD process is analyzed by changing the discharge voltage, dielectric layer material and air pressure, respectively, through the control variable method.

4.1. Discharge characteristics of particles in four cycles

In an atmosphere of pure Ar gas, the AC voltage is set to 10 kV and PTFE is taken as the dielectric layer material (relative permittivity 2.55). On this basis, the voltage and current, and electron density and electron temperature distribution are studied in one cycle to analyze the connection between them.

Figure 5 shows the voltage and current waveforms in four cycles. According to the figure, there is a one-off change in the direction of the sinusoidal AC voltage and current in one cycle, and the numerical magnitude of the voltage and current first increases and then decreases over time in the same direction as the discharge. Since the voltage and current waveforms in the four cycles are identical, the laws of electron density and electron temperature changes are studied for only one cycle in the following sections. Figure 6 shows the spatial distribution of electron density at a certain point in time. Since the electron density and electron temperature at any moment vary in each position in space, the average of electron density and electron temperature in space at each moment is taken as the electron density and electron temperature at that moment. This method is used to calculate the magnitude of electron density and electron temperature in the numerical simulation section of this paper. Figure 7 shows the variation of electron density and electron temperature in four cycles over time. As shown in the figure, electron density increases sharply and reaches its maximum in the initial stage of the discharge; this is because the electrons absorb energy and collide with Ar atoms under the action of an electric field, thus producing a large number of sub-stable Ar atoms. The density of sub-stable Ar atoms also increases rapidly. When the voltage decreases gradually, the energy absorbed by the electrons diminishes, which causes a gradual decline in the number density of sub-stable Ar atoms. During the period 80–100 μs, the particles increasingly aggregate on one side of the discharge. When the voltage is applied continuously, the energy absorbed by the electrons increases and the number of particles produced becomes larger, which means the electron density rises. In the initial stage of the discharge, the electron temperature rises at an extremely fast pace because of the energy generated after numerous electron collisions. However, in the period 60–80 μs, the energy consumed by the collisions between particles exceeds the energy released

by ionization, which reduces the electron temperature.[23] Figure 8 shows curves of the electron density and total capacitive power deposition with time. It can be seen from the figure that fluctuation of total capacitive power deposition occurs twice per cycle. The discharge process provides the energy required to excite the DBD, the discharge energy drives the generation of plasma active material in the discharge air gap and the energy is partly stored in the dielectric layer. The particles collide with each other due to the applied electric field, with a large number of free electrons and ions generated. As a result, electron density increases.

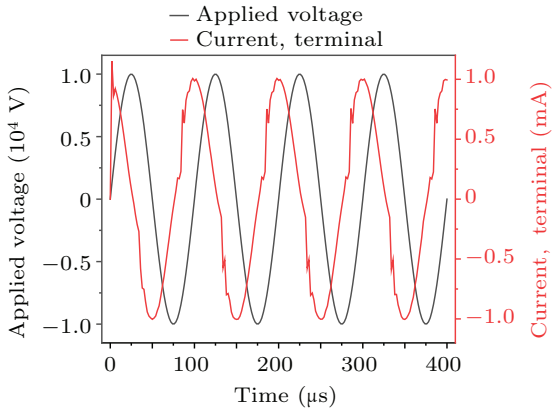


Fig. 5. Voltage and current waveforms.

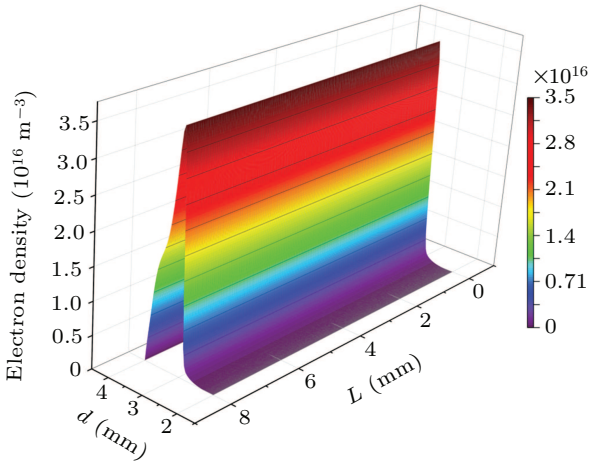


Fig. 6. Spatial distribution of electron density.

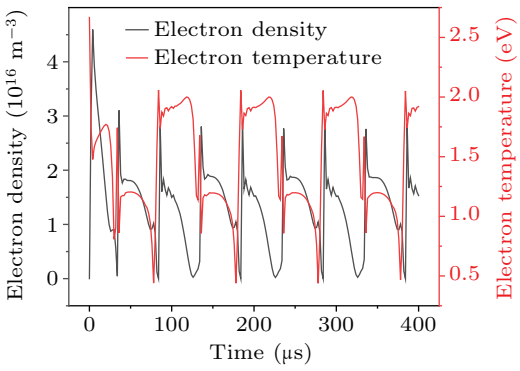


Fig. 7. Change in electron density and electron temperature.

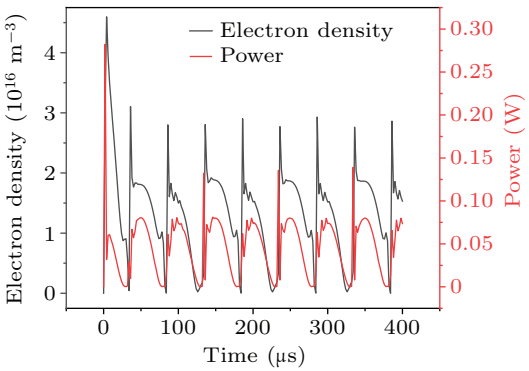


Fig. 8. Change in electron density and total capacitance power deposition.

4.2. Effect of voltage on discharge characteristics

With other conditions unchanged, a study was conducted on the effect of voltage on electron density and electron temperature when the AC voltage increases from 10 kV to 15 kV. Figure 9 shows the variation of electron density with voltage. As can be seen, the energy absorbed by the particles in the electric field increases with the gradual rise in voltage. Meanwhile, the collisions become more violent, the number of electrons produced increases and the maximum value of electron density rises from 6.36×10^{16} m^{-3} to 8.31×10^{16} m^{-3}.

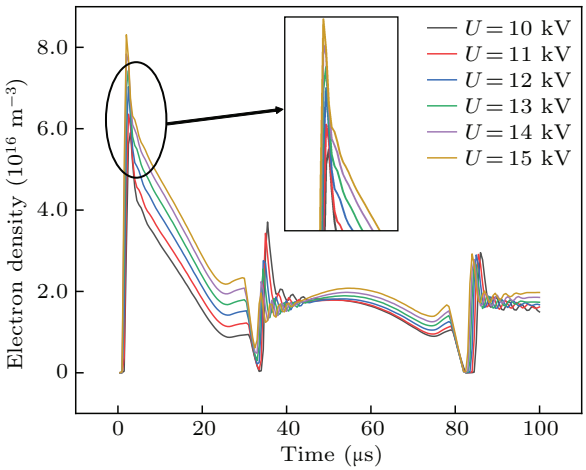


Fig. 9. Change in electron density at different voltages.

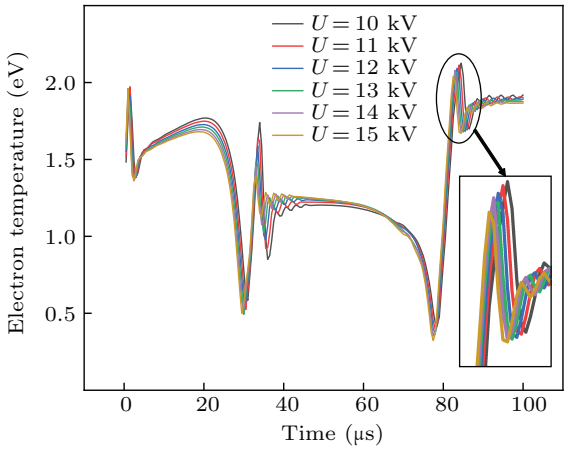


Fig. 10. Change in electron temperature at different voltages.

Figure 10 shows the change in electron temperature with voltage. As can be seen, with the increase in input voltage, the electron temperature shows an overall increasing trend and its maximum value also rises gradually. This is because the collisions between the particles absorbing energy intensifies continuously, thus leading to a rise in temperature.

4.3. Effect of dielectric layer material on discharge characteristics

With other conditions unchanged, variations of discharge characteristics were analyzed by changing the dielectric layer material. For teflon, silica and quartz as dielectric layer materials, the relative permittivities are $\varepsilon_{\text{teflon}} = 2.55$, $\varepsilon_{\text{silica}} = 3.9$ and $\varepsilon_{\text{quartz}} = 4.3$.

Figure 11 shows the variation of electron density with relative permittivity. It can be seen from the figure that the electron-dense region expands with increase in the relative permittivity. This is because when the dielectric blocks discharge, the dielectric layer acts as a capacitive element in the circuit to store the electric field energy, and the capacitance of the capacitive element increases when the relative permittivity increases. The relationship between the capacitance C, the charge q and the voltage u of the capacitive element is expressed as

$$q = Cu. \tag{14}$$

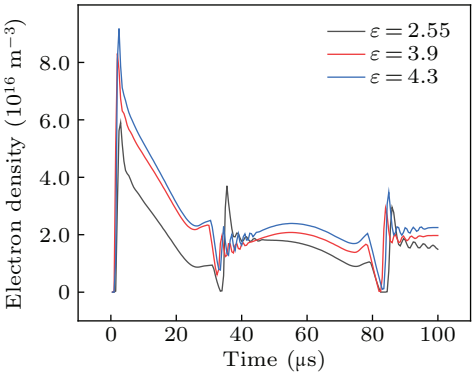


Fig. 11. Variation of electron density at different relative permittivities.

Given a certain through voltage, the larger the capacitance C, the higher the charge q and the greater the current density. Therefore, the current density increases with increase in the relative permittivity, which increases the number of charged particles on the surface of the dielectric during the discharge process, thus expanding the range of electron density distributions for which the dielectric blocks discharge. Figure 12 shows the variation of electron temperature with relative permittivity, and Fig. 13 shows the spatial distribution of electron temperature given different relative permittivities. It can be seen from the figures that the high-temperature region gradually approaches the cathode region with increase in relative permittivity, while the maximum value of electron temperature gradually decreases. This is because the intensity of electric field in the cathode region rises as the relative permittivity increases. In this case, the electrons have more energy to collide with each other, and power loss increases accordingly. Also, there is a gradual decrease not only in the width of the cathode glow region but also in the maximum value of electron temperature.

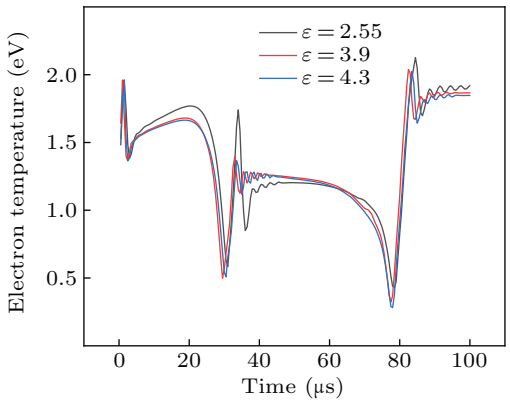


Fig. 12. Variation of electron temperature at different relative permittivities.

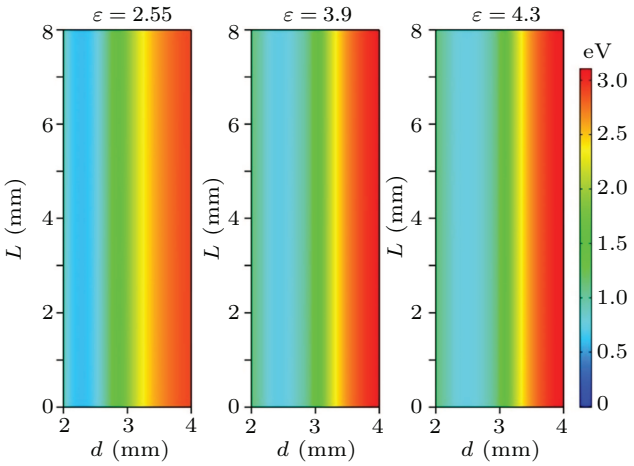


Fig. 13. Spatial distribution of electron temperature at different relative permittivities.

4.4. Effect of pressure inside the reactor on discharge characteristics

With the other parameters unchanged, the effect of air pressure on electron density and electron temperature distribution was analyzed by changing only the pressure inside the reactor. Figure 14 shows the change of electron density with discharge pressure inside the reactor. According to this figure, the electron density increases significantly when the discharge pressure inside the reactor is raised from 1.0 atm to 1.2 atm. This is because when the density of the gas rises, the free range between the particles is narrowed, the number of collisions between individual particles increases and the collision leads to the generation of more particles. That is to say, the electron density increases.

The variation of electron temperature with discharge time is shown in Fig. 15. As the discharge pressure inside reactor

increases from 1.0 atm to 1.2 atm, the electron temperature shows a decreasing trend. This is because the rise in the number of collisions between individual particles increases energy consumption, thus reducing the electron temperature.

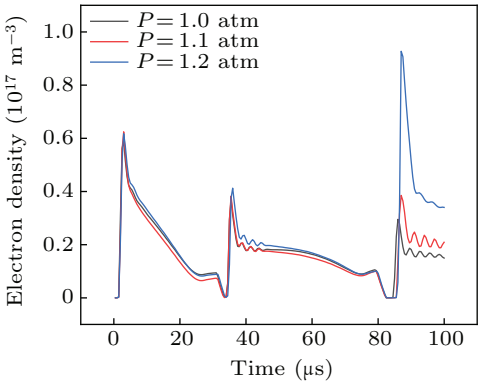


Fig. 14. Change in electron density under different pressures inside the reactor.

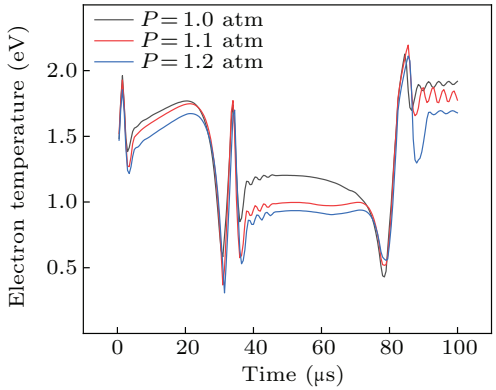


Fig. 15. Change in electron temperature under different pressures inside reactor.

4.5. Processing of experimental results

The spectral data for a DBD can be obtained by using a spectrometer and plotting a characteristic spectral map. Since the distribution of Ar atoms ranges between 680 and 850, some of the data are selected for Gaussian fitting, as shown in Fig. 16. The slope of this image is clearly observable, and has a value of $-5040/T_e$. Furthermore, the numerical magnitude of the electron excitation temperature can be obtained. With the other parameters related to the experiment kept constant, the discharge voltage is adjusted to determine the variation of electron excitation temperature with discharge voltage, as shown in Fig. 17. Through a comparison with the simulation results, it is found that the experimentally measured electron excitation temperature changes with voltage in the same way as in the simulation, so the temperature of electron excitation increases with increase in the voltage. However, there is a disparity between the experimental and simulation data due to errors in the process of experimental measurement. The errors are within the allowable range.

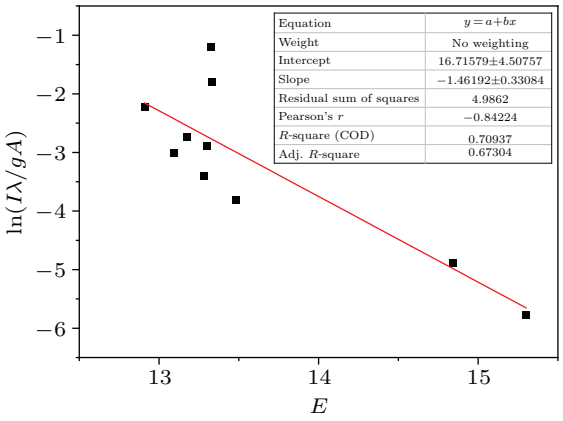


Fig. 16. Gaussian fitting diagram.

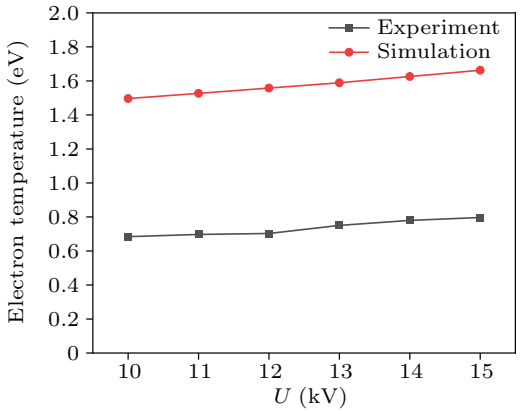


Fig. 17. Trend of changes in electron excitation temperature with voltage.

5. Conclusion

In the present work an investigation was conducted into the effects of voltage, pressure inside the reactor and dielectric layer material on the characteristics of particle discharge during the course of a coaxial dielectric blocking discharge. The main conclusions of this study are as follows.

(1) As the input voltage rises, the potential of the discharge gap increases, the particles absorb more and more energy, the collisions become intensified, the number of particles generated increases with more energy released and there is an increase in both electron density and electron temperature.

(2) With change in the dielectric layer material, the number of charged particles in the dielectric layer increases with the relative permittivity, the electron density rises and the electron temperature decreases due to the increase in energy loss caused by the collisions.

(3) With a gradual rise in pressure inside reactor, the gas density increases, which causes the number of particle collisions to increase. Meanwhile, the electron density increases, while the electron temperature gradually declines due to energy consumption between the particles.

Acknowledgements

Project supported by the National Natural Science Foundation of China (Grant Nos. 51509035 and 51409158), the

Project of Shenyang Science and Technology Bureau (Grant No. RC200010), and the National Natural Science Foundation of Liaoning Province of China (Grant No. 2020-KF-13-03).

References

[1] Mustafa A, Lougou B G, Shuai Y, Wang Z J and Tan H P 2020 *Journal of Energy Chemistry.* **49** 96
[2] Kogelschatz U 2003 *Plasma Chemistry and Plasma Processing* **23** 1
[3] Zhang Y T, Wang D Z and Wang Y H 2005 *Phys. Plasmas* **12** 103508
[4] Wang X X 2009 *High Volatage Engineering* **34** 1
[5] Na N, Zhao M, Zhang S, Yang C D and Zhang X R 2007 *Journal of the American Society for Mass Spectrometry* **18** 1859
[6] Kogelschatz U 2003 *Plasma Chemistry and Plasma Processing* **23** 1
[7] Massine F and Gouda G A 1999 *J. Phys. D Appl. Phys.* **31** 3411
[8] Li X, Zhang Q, Chu J, Li J and Jia P 2017 *High Voltage Engineering.* **43** 1880
[9] Ding X and Duan Y 2015 *Mass Spectrometry Reviews* **34** 449
[10] Roth J R 2003 *Phys. Plasmas* **10** 2117
[11] Wu Y and Li Y 2015 *Acta Aeronautica et Astronautica Sinica* **36** 381
[12] Saifutdinova A A, Timerkaev B A and Saifutdinov A I 2019 *J. Phys. Conf. Series* **1328** 012082
[13] Judée F, Merbahi N, Wattieaux G and Yousfi M 2016 *J. Appl. Phys.* **120** 114901
[14] Barkaoui G, Halima A B, Jomaa N, Charrada K and Yousfi M 2021 *IEEE Transactions on Plasma Science* **49** 1302
[15] Bai C, Wang L, Li L, Dong X, Xiao Q, Liu Z, Sun J and Pan J 2019 *AIP Advances* **9** 035023
[16] Wang J, Lei B, Li J, Xu Y, Wang Y, Tang J, Zhao W and Duan Y 2020 *Phys. Plasmas* **27** 043501
[17] Wang C, Yao C, Chang Z and Zhang G 2019 *Phys. Plasmas* **26** 123506
[18] Saifutdinova A A, Timerkaev B A and Saifutdinov A I 2019 *J. Phys. Conf. Series* **1328** 012082
[19] Stenzel R L 1988 *Phys. Rev. Lett.* **60** 704
[20] Shi J J amd Kong M G 2005 *Appl. Phys. Lett.* **87** 201501
[21] Chirokov A, Khot S N, Gangoli S P, Fridman1 A, Henderson P, Gutsol A F and Dolgopolsky A 2009 *Plasma Sources Science & Technology* **18** 025025
[22] Hagelaar M and Pitchford C 2005 *Plasma Sources Science and Technology* **14** 722
[23] Li P, Xu J, Chen Z and Xu G 2020 *High Voltage Apparatus* **56** 173